When it is on, adipogenesis is repressed; when it is off, adipogenesis is initiated. The crucial role of Wnt signaling in the adipogenic program is emphasized by the finding that in its absence, myoblasts are reprogrammed to the adipocyte lineage and undergo spontaneous differentiation.

**References and Notes**


1. P. Cornelius, O. A. MacDougald, M. D. Lane, *Annu. Rev. Nutr.* **14**, 99 (1994).
2. O. A. MacDougald and M. D. Lane, *Annu. Rev. Biochem.* **64**, 345 (1995).
3. G. J. Darlington, S. E. Ross, O. A. MacDougald, *J. Biol. Chem.* **273**, 30057 (1998).
4. B. M. Spiegelman, *Diabetes* **47**, 507 (1998).
5. K. M. Cadigan and R. Nusse, *Genes Dev.* **11**, 3286 (1997).
6. A. Kikuchi, *Cytokine Growth Factor Rev.* **10**, 255 (1999).
7. J. R. Miller, A. M. Hocking, J. D. Brown, R. T. Moon, *Oncogene* **18**, 7860 (1999).
8. A. Bafico, A. Gazit, S. S. Wu-Morgan, A. Yaniv, S. A. Aaronson, *Oncogene* **16**, 2819 (1998).
9. P. S. Klein and D. A. Melton, *Proc. Natl. Acad. Sci. U.S.A.* **93**, 8455 (1996).
10. F. T. Kolligs, G. Hu, C. V. Dang, E. R. Fearon, *Mol. Cell. Biol.* **19**, 5696 (1999).
11. C. S. Young, M. Kitamura, S. Hardy, J. Kitajewski, *Mol. Cell. Biol.* **18**, 2474 (1998).
12. S. E. Ross, N. Hemati, O. A. MacDougald, data not shown.
13. H. Green and O. Kehinde, *J. Cell. Physiol.* **101**, 169 (1979).
14. S. Mandrup, T. M. Loftus, O. A. MacDougald, F. P. Kuhajda, M. D. Lane, *Proc. Natl. Acad. Sci. U.S.A.* **94**, 4300 (1997).
15. Although Wnt-1 is a mitogen in many cell types and caused elevated cyclin D1 in 3T3-L1 preadipocytes, its expression did not alter the number of cells at confluence or during MDI-induced clonal expansion, nor did it cause an elevation in c-Myc protein.
16. N.-d. Wang *et al.*, *Science* **269**, 1108 (1995).
17. B. B. Lowell, *Cell* **99**, 239 (1999).
18. D. Shao and M. A. Lazar, *J. Biol. Chem.* **272**, 21473 (1997).
19. V. Korinek *et al.*, *Science* **275**, 1784 (1997).
20. M. A. Julius *et al.*, in preparation.
21. S. Hoppler, J. D. Brown, R. T. Moon, *Genes Dev.* **10**, 2805 (1996).
22. G. Cossu and U. Borello, *EMBO J.* **18**, 6867 (1999).
23. Primers and PCR reactions were as described in (*24*). A second PCR reaction was performed with a sense primer that is one nucleotide shorter at the 3′ end. PCR products were analyzed on agarose gels, cloned into pCR II (Invitrogen, Carlsbad, CA) and sequenced.
24. J. L. Christian, B. J. Gavin, A. P. McMahon, R. T. Moon, *Dev. Biol.* **143**, 230 (1991).
25. A. D. Miller and G. J. Rosman, *Biotechniques* **7**, 980 (1989).
26. N. Hemati, S. E. Ross, R. L. Erickson, G. E. Groblewski, O. A. MacDougald, *J. Biol. Chem.* **272**, 25913 (1997).
27. S. E. Ross, R. L. Erickson, N. Hemati, O. A. MacDougald, *Mol. Cell. Biol.* **19**, 8433 (1999).
28. F.-T. Lin, O. A. MacDougald, A. M. Diehl, M. D. Lane, *Proc. Natl. Acad. Sci. U.S.A.* **90**, 9606 (1993).
29. P. Tontonoz, E. Hu, B. M. Spiegelman, *Cell* **79**, 1147 (1994).
30. D. J. Van Den Berg, A. K. Sharma, E. Bruno, R. Hoffman, *Blood* **92**, 3189 (1998).
31. O. A. MacDougald, C.-S. Hwang, H. Fan, M. D. Lane, *Proc. Natl. Acad. Sci. U.S.A.* **92**, 9034 (1995).
32. E. A. Cho and G. R. Dressler, *Mech. Dev.* **77**, 9 (1998).


33. We thank M. A. Lazar, J. Kitajewski, E. Fearon, D. J. Van Den Berg, and G. Dressler for plasmids; D. A. Bernlohr for antibody to 422/aP2; and K. Cadigan, C. Carter-Su, K. L. Guan, E. Fearon, and J. Williams for critical review of the manuscript. Supported in part by grants from the NIH (RO1-DK51563 to O.A.M.), the Natural Sciences and Engineering Research Council of Canada (S.E.R. and R.L.E.), the University of Michigan Endocrinology and Metabolism Fellowship Training Grant T32-DK07245 (K.A.L.), and the Michigan Diabetes Research and Training Center (NIH 5P60 DK20572).

9 June 2000; accepted 26 June 2000


# Calcium Sensitivity of Glutamate Release in a Calyx-Type Terminal


**Johann H. Bollmann,[1]* Bert Sakmann,[1] J. Gerard G. Borst[1,2]**



**Synaptic efficacy critically depends on the presynaptic intracellular calcium concentration ($[Ca^{2+}]_i$). We measured the calcium sensitivity of glutamate release in a rat auditory brainstem synapse by laser photolysis of caged calcium. A rise in $[Ca^{2+}]_i$ to 1 micromolar readily evoked release. An increase to >30 micromolar depleted the releasable vesicle pool in <0.5 millisecond. A comparison with action potential–evoked release suggested that a brief increase of $[Ca^{2+}]_i$ to ~10 micromolar would be sufficient to reproduce the physiological release pattern. Thus, the calcium sensitivity of release at this synapse is high, and the distinction between phasic and delayed release is less pronounced than previously thought.**


In response to an action potential, the presynaptic release probability is strongly increased for a few milliseconds. This phasic release is thought to be triggered by a brief, localized increase in $[Ca^{2+}]_i$ in the vicinity of open, presynaptic $Ca^{2+}$ channels. The $Ca^{2+}$ sensitivity of phasic release in mammalian central synapses is not yet known. On the basis of results obtained in other synapses, it has been assumed that a low-affinity $Ca^{2+}$ sensor, which is activated by local increases of $[Ca^{2+}]_i$ to >100 μM, triggers phasic release in mammalian central synapses (*1–4*). In contrast, the more prolonged, delayed release period that, at most synapses, follows the phasic release may be controlled by a separate $Ca^{2+}$ sensor with a much higher affinity for $Ca^{2+}$ (*5*).

We measured the $Ca^{2+}$ sensitivity of glutamate release at a giant synapse in the auditory brainstem, the axosomatic synapse formed by the calyx of Held with a principal cell in the medial nucleus of the trapezoid body. Using laser photolysis of caged $Ca^{2+}$, we compared in the same terminals release evoked by a sustained, spatially uniform rise in presynaptic $[Ca^{2+}]_i$ (*6*) with release triggered by action potentials, during which changes in $[Ca^{2+}]_i$ are transient and highly localized (*3*). In 9-day-old rats, this synapse shows prominent synaptic depression during high-frequency signaling, which is most likely caused by rapid depletion of the releasable pool of vesicles (*6–8*). In order to relate the flash-evoked excitatory postsynaptic currents (EPSCs) to the size of the releasable pool in the same terminal, we first estimated the releasable pool size in the intact terminal. Simultaneous pre- and postsynaptic recordings were made from the calyx and a principal cell (*9*). With the presynaptic recording still in the cell-attached configuration, a train of action potentials was evoked by an extracellular electrode (Fig. 1A). A measure of release was obtained from the amplitudes of the glutamatergic EPSCs simultaneously recorded in the principal cell. During the train, the size of the EPSCs rapidly depressed, reaching a steady state within 100 ms. The cumulative amplitude of the EPSCs evoked by a train of afferent stimuli (200 ms, 200 Hz) was taken as a measure of the size of the releasable pool (*7*). This estimate was corrected for the steady-state component in the EPSCs (Fig. 1B). The cumulative EPSC was −9.7 ± 0.7 nA ($n$ = 43, mean ± SEM) at a holding potential of −30 mV. The quantal EPSC amplitude was −32 ± 2 pA ($n$ = 10 cells) at −80 mV. Assuming that the release of one vesicle gives an EPSC amplitude of −12 pA at −30 mV, this gave a releasable pool size of 810 ± 60 vesicles (*6*, *7*). The amplitude of the first EPSC was 21 ± 2% ($n$ = 43) of the amplitude of the cumulative EPSC. Taking the decay of the quantal EPSC into account, this means that about one-quarter of the releasable vesicle pool is released by a single action potential. In the presence of cyclothiazide, the 20 to 80% rise time of a single action potential–evoked EPSC was 424 ± 11 μs ($n$ = 43). Its time course was not different at holding potentials of −80 and −30 mV (paired $t$ test, $P$ > 0.05; $n$ = 7).

After establishing the whole-cell configuration, the terminal was loaded via the patch


[1]Max-Planck-Institute for Medical Research, Department of Cell Physiology, Jahnstrasse 29, D-69120 Heidelberg, Germany. [2]Swammerdam Institute for Life Sciences, University of Amsterdam, Kruislaan 320, 1098 SM Amsterdam, the Netherlands.

*To whom correspondence should be addressed. E-mail: jbollman@mpimf-heidelberg.mpg.de

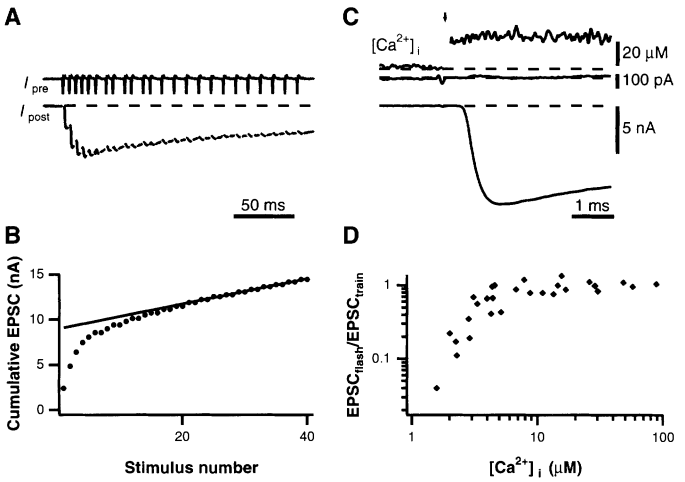


**Fig. 1.** Rapid depletion of the releasable vesicle pool by $[Ca^{2+}]_i$ jumps. Data in (A) to (C) are from the same synapse. **(A)** A high-frequency train of afferent stimuli induced presynaptic action potentials ($I_{pre}$, presynaptic cell-attached voltage-clamp recording) and EPSCs ($I_{post}$, postsynaptic whole-cell voltage-clamp recording). Vertical scaling as in (C). Postsynaptic holding potential was −30 mV. Stimulus artifacts have been removed. **(B)** The peak-to-peak amplitudes of the individual EPSCs shown in (A) were summed (●) to estimate the releasable pool size in the intact terminal. The solid line is a linear regression of the steady-state component of the train. Back-extrapolation to the start of the train gave an estimate for the cumulative amplitude of the train in the absence of pool replenishment (*6*). **(C)** After presynaptic whole-cell dialysis, a UV laser pulse (arrow) evoked a rapid and sustained $[Ca^{2+}]_i$ increase (top trace) to 26 μM. The increase in $[Ca^{2+}]_i$ resulted in a rapid, large EPSC (bottom trace), whose amplitude approximated the (corrected) sum of the amplitudes of the EPSC train in (A). Its amplitude was larger and its rise time was faster than the action potential–evoked EPSC in the same terminal. Pre- and postsynaptic holding potentials were −80 and −30 mV, respectively. **(D)** Relative size of the EPSC evoked by the UV flash compared with the cumulative EPSC amplitude evoked by afferent trains in the same terminals, displayed on log-log coordinates. Data were pooled from 26 experiments.

pipette with a solution containing the ultraviolet (UV)-sensitive $Ca^{2+}$ buffer DM-nitrophen (DM-n) (*10*) and a low-affinity $Ca^{2+}$ indicator. This enabled us to evoke transmitter release by rapidly uncaging $Ca^{2+}$ by laser photolysis of DM-n (*11–13*). The spatially uniform rise in $[Ca^{2+}]_i$ to levels between 0.5 and 100 μM was monitored with a photodiode (Fig. 1C), starting ~200 μs after the UV pulse. At this point, the rapid decay component of the transient $[Ca^{2+}]_i$ spike (*11*, *14*) had already subsided (*15*). The measured $[Ca^{2+}]_i$ decayed by about 30% in 50 ms. The increase in $[Ca^{2+}]_i$ induced a small, slow outward current in the presynaptic terminal that was not further investigated. Laser photolysis triggered EPSCs, whose amplitude depended on the $[Ca^{2+}]_i$ levels that were reached. Increases in $[Ca^{2+}]_i$ to concentrations of 7 μM and higher evoked an EPSC with an amplitude that was as large as the cumulative amplitude of the EPSCs evoked by the brief afferent stimulus train before the whole-cell configuration was established (Fig. 1D). At lower $[Ca^{2+}]_i$ the laser-evoked EPSCs were smaller (Figs. 1D and 2A), probably because of the decay of the quantal EPSCs during the rising phase of these slower EPSCs. Therefore, our results suggest that the measured increases in $[Ca^{2+}]_i$ after laser photolysis targeted the same, kinetically distinct, pool of vesicles as released by the transient, localized increase in $[Ca^{2+}]_i$ after an action potential (*6*).

We estimated the release rate per single vesicle after a $[Ca^{2+}]_i$ jump. Larger increases in $[Ca^{2+}]_i$ evoked EPSCs with a smaller delay and a shorter rise time (Fig. 2A). Apparently, the time needed to deplete the releasable pool depended on $[Ca^{2+}]_i$, suggesting that a sustained increase in $[Ca^{2+}]_i$ of >4 μM was sufficient to deplete the releasable pool of vesicles on a millisecond time scale. The rising phase of the compound EPSCs could therefore be used to calculate release rates (*16*). The peak release rate during a laser-evoked EPSC was divided by the estimated number of releasable vesicles for the same synapse, thus correcting for pool size variability between synapses. In contrast to results obtained in other preparations (*17*, *18*), there was no clear threshold for transmitter release. $[Ca^{2+}]_i$ increases to ~1 μM, which is close to the $[Ca^{2+}]_i$ during the delayed release phase in the calyx of Held (*19*), triggered a sequence of individually resolvable quantal EPSCs (Fig. 2B). Their frequency provided a direct measure of the evoked change in release rate. The calculated release rate varied more than 10,000-fold as $[Ca^{2+}]_i$ varied from 0.5 to 100 μM (Fig. 2C) (*20*, *21*). The fastest rise times of the laser-evoked EPSCs measured were 220 ± 12 μs ($n$ = 4), corresponding to a maximal release rate of ~6 $ms^{-1}$ per vesicle. The delay from the UV pulse to the start of the EPSC was less than 0.3 ms at a $[Ca^{2+}]_i$ of >30 μM, whereas at a $[Ca^{2+}]_i$ of ~1 μM, the delay to the first quantal EPSC was still on average <10 ms (Fig. 2D). This indicates that the $Ca^{2+}$ sensor binds $Ca^{2+}$ rapidly before it triggers the final steps of transmitter release.

We fitted the relation between peak release rate and $[Ca^{2+}]_i$ using a kinetic model of the $Ca^{2+}$ sensor and its interaction with the releasable vesicles (Fig. 2C). The model features five identical $Ca^{2+}$-binding steps, followed by a final, reversible, $Ca^{2+}$-independent isomerization step that promoted vesicle fusion (*22*). A satisfactory prediction of the $[Ca^{2+}]_i$ dependence of both the release rates and the delays was obtained with the parameters given in (*22*). Although this parameter set was not unique, several conclusions could be drawn from the fitting procedure. To reproduce the fast depletion of the pool at high $[Ca^{2+}]_i$, a large isomerization rate constant and fusion rate constant were needed. To reproduce the apparent saturation of release rates at $[Ca^{2+}]_i$ of >30 μM, a dissociation constant ($K_d$) of ~10 μM for the individual binding steps was needed, not very different from the estimated affinities of the $Ca^{2+}$ sensor that triggers the release of large dense-core vesicles (*23–25*), but clearly lower than previously estimated for the release of clear vesicles from bipolar cells of the goldfish retina (*26*).

The laser photolysis experiments can be used to calculate the typical $[Ca^{2+}]_i$ transient observed by a $Ca^{2+}$ sensor during action potentials (*27*). The rise times of the action potential–evoked EPSCs indicated that peak release rates were 0.42 ± 0.04 $ms^{-1}$ per vesicle ($n$ = 43). A sustained increase of $[Ca^{2+}]_i$ to 5 μM gave release rates similar to the ones observed during action potentials (Fig. 3A). This concentration is therefore a lower estimate, because the peak $[Ca^{2+}]_i$ reached during an action potential will be reached only very briefly and will not trigger release as efficiently as a steady increase to the same level.

An upper estimate can be obtained for the $[Ca^{2+}]_i$ transient peak value for the hypothetical situation that all release sites faced the same $[Ca^{2+}]_i$ transient. We assumed that the time course of the $[Ca^{2+}]_i$ transient at the $Ca^{2+}$ sensor is not faster than the $Ca^{2+}$ current during an action potential (Fig. 3B), which was measured previously (*22*, *28*). With this time course, the amount of release evoked by the simulated $[Ca^{2+}]_i$ transient matched the release evoked by real action potentials if the peak $[Ca^{2+}]_i$ was ~9 μM. This estimate was largely model-independent. After adjustment of the parameters of other kinetic models (*24*, *26*, *29*) to satisfy the relation between $[Ca^{2+}]_i$ and release rates, a similar estimate was obtained (*30*). Assuming a linear relation between $Ca^{2+}$ influx and the peak of the $[Ca^{2+}]_i$ transient, the simulated action potential–evoked release shared several features with the experimentally characterized release. Delays and rise times of EPSCs were largely independent of the amount of $Ca^{2+}$ influx during the action potential (*28*), although for very high $Ca^{2+}$ influx, a decrease in the

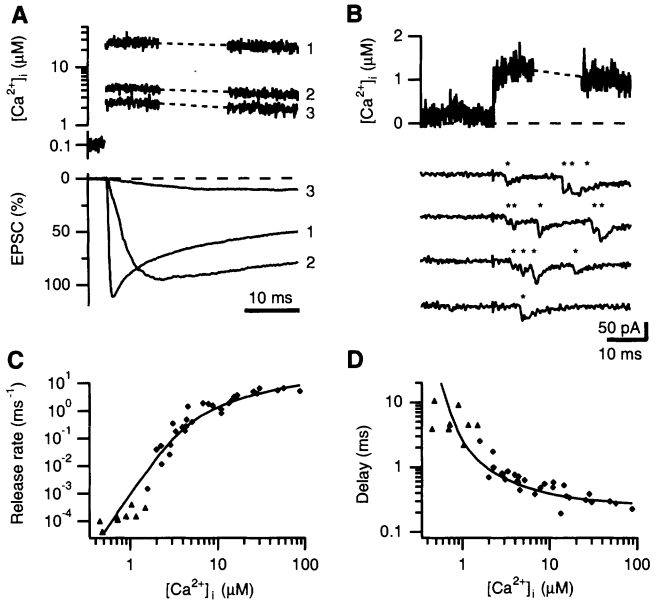


**Fig. 2.** Relation between $[Ca^{2+}]_i$ and the rate of exocytosis in the calyx of Held. **(A)** (Top) Photodiode traces of $[Ca^{2+}]_i$ jumps to 26 (trace 1), 4.5 (trace 2), and 2.3 μM ( trace 3) in three different experiments. During the period indicated by the horizontal dashed lines, the excitation wavelength was briefly switched to the isosbestic wavelength. (Bottom) Corresponding postsynaptic currents. EPSCs were normalized to the size of the cumulative EPSC amplitude obtained in the same experiment. **(B)** A uniform increase of the $[Ca^{2+}]_i$ in the terminal to <1.5 μM (top) resulted in a clear increase in the frequency of small EPSCs (bottom traces, $V_h$ = −80 mV). UV pulses were separated by ~3 min. (Top) Overlaid $[Ca^{2+}]_i$ of the first and the last of four sweeps. (Bottom) Asterisks mark putative quantal release events. **(C)** Summary of the relation between peak release rates and $[Ca^{2+}]_i$, displayed on log-log coordinates. Peak release rates of compound EPSCs (◆) were corrected for the finite rise time of the average quantal EPSC. For $[Ca^{2+}]_i$ jumps of <1.5 μM, the average quantal EPSC rate (▲) was analyzed during the 20 ms after the mean first latency in three to five sweeps per experiment. The solid line is derived from a kinetic model of the $Ca^{2+}$ sensor (*22*). The measured relation between release rate and $[Ca^{2+}]_i$ followed a power dependence of 4.4 for $[Ca^{2+}]_i$ of <5 μM. Release rates are specified per vesicle. Data of 31 synapses were pooled. **(D)** $[Ca^{2+}]_i$ dependence of the delays between the $[Ca^{2+}]_i$ jump and the onset of release. The onset of compound release (◆) was defined as the time when the EPSC intersected a threshold of −35 pA; the onset of quantal release (▲) was defined as the mean first latency of the quantal EPSCs. Solid line, the predicted mean delay between the $[Ca^{2+}]_i$ jump and the release of the first transmitter quantum. A delay of 250 μs was added to the simulated delays to match the experimental data (*48*).

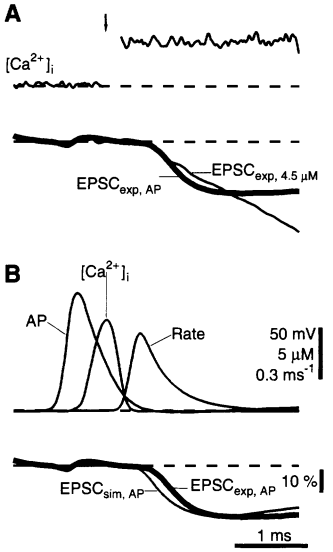


**Fig. 3.** Comparison of release rates after action potentials and $[Ca^{2+}]_i$ jumps. **(A)** A prolonged $[Ca^{2+}]_i$ increase to 4.5 μM (top) evoked an EPSC ($EPSC_{exp,\ 4.5\ \mu M}$, bottom) that rises almost as fast as an action potential–evoked EPSC ($EPSC_{exp,\ AP}$). The action potential–evoked EPSC was aligned such that the putative peak of the presynaptic $Ca^{2+}$ current coincided with the $[Ca^{2+}]_i$ jump (arrow). Scaling as in (B). **(B)** Simulation of EPSCs evoked by a brief increase in $[Ca^{2+}]_i$. The time course of the $[Ca^{2+}]_i$ transient was assumed to be the same as that of the measured $Ca^{2+}$ current during an action potential (top) (*22*). It was scaled and used to drive the kinetic release model to simulate a release rate (Rate) that produced an EPSC ($EPSC_{sim,\ AP}$) of the same amplitude as observed during action potential–evoked release ($EPSC_{exp,\ AP}$). The simulated release rate and EPSC were shifted to the right by 250 μs (*48*).

synaptic delay and the rise time was observed. The time course of the release probability matched the experimentally observed time course (*28*). The model predicted a fourth-power dependence of EPSC amplitudes on external $[Ca^{2+}]$, somewhat higher than previously measured (*6*). Our results do not indicate that $Ca^{2+}$ sensors never experience $[Ca^{2+}]_i$ of >10 μM during action potentials. However, they suggest that, in contrast to earlier suggestions (*1–4*), most $Ca^{2+}$ sensors in the calyx of Held do not experience $[Ca^{2+}]_i$ of hundreds of μM, because even if they were exposed for a brief period, release during action potentials would be faster and larger than experimentally observed.

We conclude that transmitter release from the calyx of Held exhibited a high $Ca^{2+}$ sensitivity compared with previous estimates for the release of clear vesicles from other synapses (*18*, *26*). Our characterization of the $Ca^{2+}$ sensitivity of synaptic transmitter release may be of use in identifying possible $Ca^{2+}$ sensors and in elucidating the molecular mechanisms of transmitter release. For example, synaptotagmin I and II are prominent candidates for the $Ca^{2+}$ sensor that triggers phasic release (*2*, *4*). Our results suggest that its binding to syntaxin is unlikely to be involved in the final steps before fusion at the calyx of Held because it requires very high $[Ca^{2+}]_i$ (*2*). Synaptic terminals contain a plethora of other $Ca^{2+}$-binding proteins with a higher affinity for $Ca^{2+}$, which may be considered as alternative candidates for the $Ca^{2+}$ sensor (*4*).

We recorded from calyces of young rats, and the $Ca^{2+}$ sensitivity of release may change during development. However, the observed high sensitivity agrees with other observations. First, $[Ca^{2+}]_i$ of <10 μM evoke substantial release in the squid giant synapse (*31*, *32*) and in the crayfish neuromuscular junction (*33*). Second, the slow $Ca^{2+}$ buffer EGTA not only abolishes delayed release (*28*, *34*, *35*), but also affects phasic release at many synapses (*28*, *34*, *36*). $[Ca^{2+}]_i$ of hundreds of μM are reached only in the immediate vicinity of open $Ca^{2+}$ channels, where EGTA would be ineffective. Third, at the frog neuromuscular junction, EGTA inhibits release, but not the $Ca^{2+}$-dependent potassium channels. This suggests that the $Ca^{2+}$ sensor for release is farther away from the $Ca^{2+}$ channels than the $Ca^{2+}$-dependent potassium channels (*37*). At the cultured neuromuscular junction, simulations suggest that $[Ca^{2+}]_i$ is <10 μM in most regions of a presynaptic $Ca^{2+}$ entry site (*38*). Combined with our result that a low-affinity $Ca^{2+}$ sensor is not a prerequisite for phasic transmitter release, these results suggest that the high $Ca^{2+}$ sensitivity of phasic release at the calyx of Held may be a property of many synapses.

The phasic-release $Ca^{2+}$ sensor equilibrated rapidly to changes in $[Ca^{2+}]_i$ and triggered release with a high maximal speed, much faster than for dense-core vesicles (*39*). However, the $Ca^{2+}$ sensitivity observed in the calyx was not very different from the sensitivity of the release of large dense-core vesicles in, for example, melanotrophs (*23*). Similar $Ca^{2+}$-binding mechanisms may therefore be at work. Finally, because the $Ca^{2+}$ sensor that triggers phasic release has relatively high $Ca^{2+}$ sensitivity, it may be predicted that delayed release is to a large extent a consequence of a delayed triggering of the same sensor, rather than a result of the triggering of a different sensor with much higher affinity.

### References and Notes

1. G. J. Augustine, E. M. Adler, M. P. Charlton, *Ann. N.Y. Acad. Sci.* **635**, 365 (1991).
2. T. C. Südhof and J. Rizo, *Neuron* **17**, 379 (1996).
3. E. Neher, *Neuron* **20**, 389 (1998).
4. R. D. Burgoyne and A. Morgan, *Cell Calcium* **24**, 367 (1998).
5. R. S. Zucker, *Curr. Opin. Neurobiol.* **9**, 305 (1999).
6. R. Schneggenburger, A. C. Meyer, E. Neher, *Neuron* **23**, 399 (1999).

7. L.-G. Wu and J. G. G. Borst, *Neuron* **23**, 821 (1999).
8. H. von Gersdorff, R. Schneggenburger, S. Weis, E. Neher, *J. Neurosci.* **17**, 8137 (1997).


9. Transverse brainstem slices were cut from 8- to 10-day-old Wistar rats with a vibratome. The extracellular recording solution contained (in mM) 125 NaCl, 2.5 KCl, 1 $MgCl_2$, 2 $CaCl_2$, 25 dextrose, 1.25 $NaH_2PO_4$, 0.4 ascorbic acid, 3 *myo*-inositol, 2 sodium pyruvate, and 25 $NaHCO_3$ (bubbled with 5% $CO_2$, 95% $O_2$). Postsynaptic *N*-methyl-D-aspartate receptors were blocked by D-2-amino-5-phosphonovalerate (50 μM). Cyclothiazide (CTZ, 100 μM) was added to minimize postsynaptic AMPA receptor desensitization. Simultaneous pre- and postsynaptic whole-cell recordings from giant synapses (*40*) were made with two Axopatch 200B amplifiers. Recordings were made at room temperature. The postsynaptic pipette solution contained (in mM) 125 cesium gluconate, 20 CsCl, 10 disodium phosphocreatine, 4 MgATP, 0.3 guanosine 5′-triphosphate (GTP), 10 Hepes, 0.5 EGTA (pH 7.2). The presynaptic pipette solution contained (in mM) 90 potassium gluconate, 20 KCl, 30 Hepes, 9 DM-nitrophen (DM-n, Calbiochem, CA), ~8.6 $CaCl_2$ (pH 7.2). Either Mag-fura-2 or Fura-2FF was added as low-affinity $Ca^{2+}$ indicators (1 mM). We confirmed on each experimental day that the $[Ca^{2+}]_i$ of this solution was ~100 nM, using Fura-2 (0.2 mM). For $[Ca^{2+}]_i$ jumps to <6 μM and unless MgATP was included (*20*), the [DM-n] was lowered to 5 or 2.5 mM and the [$CaCl_2$] proportionately to reduce the rebinding of $Ca^{2+}$ to unphotolyzed DM-n. Postsynaptic pipettes had an open-tip resistance of 2 to 3 megohm. The uncompensated series resistance was 12 ± 1 megohm ($n$ = 43), electronically compensated to 90 to 95%. The recorded EPSCs were corrected off-line for the voltage error caused by the residual series resistance (*41*). Presynaptic pipettes (4 to 6 megohm) dialyzed the terminal for at least 4 min before a laser pulse was applied. All compound EPSCs and spontaneous quantal EPSCs were filtered at 5 kHz (4-pole Bessel filter), digitized, stored, and analyzed as in (*28*). Quantal release events after $[Ca^{2+}]_i$ jumps to <1.5 μM were filtered at 2 kHz (Fig. 2B), in some experiments after wash-out of CTZ.


10. J. H. Kaplan and G. C. Ellis-Davies, *Proc. Natl. Acad. Sci. U.S.A.* **85**, 6571 (1988).
11. A. L. Escobar *et al.*, *Pflügers Arch.* **434**, 615 (1997).
12. G. C. Ellis-Davies, J. H. Kaplan, R. J. Barsotti, *Biophys. J.* **70**, 1006 (1996).


13. UV pulses from a frequency-tripled yttrium-aluminum-garnet–Nd laser were coupled into the epifluorescence port of an Axioskop by means of a quartz light guide and combined with the light of a monochromator. An area of 30 μm by 30 μm in the specimen plane was homogeneously illuminated by the laser pulse. The pulse intensity was attenuated by insertion of neutral density filters. A photodiode was used to record the fluorescence from dialyzed terminals. The photocurrent was amplified with an Axopatch 200A amplifier (*11*), filtered, and sampled at the same frequency as the whole-cell current recordings. UV illumination at 380/341 nm and 380/352 nm was used for dual-wavelength excitation of Mag-fura-2 and Fura-2FF, respectively. Background luminescence following a UV laser pulse was recorded after each experiment and subtracted off-line. To calibrate the $[Ca^{2+}]_i$ measurement, we determined ratiometric constants ($R_{min}$, $R_{max}$) in presynaptic terminals in separate experiments [Mag-fura-2: $R_{min}$ = 0.358 ± 0.007, $R_{max}$ = 4.61 ± 0.52; Fura-2FF: $R_{min}$ = 0.734 ± 0.010, $R_{max}$ = 6.23 ± 0.27 ($n$ = 5 for each value)]. The $[Ca^{2+}]_i$ measurement critically depends on the in situ $K_d$ of the used $Ca^{2+}$ indicators. Reported values range from 23 to 100 μM for Mag-fura-2 and 5 to 35 μM for Fura-2FF. We determined the $K_d$ of the indicators in presynaptic terminals with a similar solution as in (*9*), but with the free $[Ca^{2+}]_i$ buffered to 32 and 14 μM, respectively, using 1,3-diamino-2-hydroxypropane-tetraacetic acid [25 mM, $K_d$ = 81 μM (*42*)]. The $K_d$'s of Mag-fura-2 and of Fura-2FF were 31 ± 3 μM ($n$ = 9) and 8.9 ± 0.6 μM ($n$ = 6), respectively. The photolysis rate by monochromator UV light was ~0.07 $s^{-1}$, which did not appreciably increase basal $[Ca^{2+}]_i$ before the flash. UV pulses in the absence of a presynaptic recording did not affect the size of the afferently evoked EPSCs ($n$ = 4).


14. R. S. Zucker, *Cell Calcium* **14**, 87 (1993).


15. The kinetics of the photolysis reaction and the rebinding of $Ca^{2+}$ to unphotolyzed DM-n can lead to a rapidly decaying $[Ca^{2+}]_i$ spike (*11*, *12*, *14*). At a concentration of 1 mM, the low-affinity dyes Mag-fura-2 and Fura-2FF act as potent buffers of μM concentrations of $Ca^{2+}$ and, owing to their fast kinetics, should mirror the $[Ca^{2+}]_i$ time course with delays of a few hundred μs. In the ~200 μs after a laser pulse, the fluorescence signal was unreliable because of luminescence in the optical path. We simulated the photolysis kinetics, similar to a previous model (*11*). It reported a $[Ca^{2+}]_i$ overshoot of <100-μs duration that could exceed the measured $[Ca^{2+}]_i$ by <500% (for Fura-2FF, assumed $k_{on}$ = 0.55 $\mu M^{-1}$ $ms^{-1}$) or <50% [for Mag-fura-2, $k_{on}$ = 0.75 $\mu M^{-1}$ $ms^{-1}$ (*43*)]. Adenosine 5′-triphosphate (ATP) and endogenous $Ca^{2+}$ buffers were not taken into account, which should further dampen the initial $[Ca^{2+}]_i$ spike. The $[Ca^{2+}]_i$ spike is a function of, for example, the photolysis efficiency (1 to 14% in our experiments) and $[Ca^{2+}]_i$ buffer conditions (*11*). In our experiments, release rates observed at similar measured $[Ca^{2+}]_i$ levels, but with different buffer conditions and photolysis efficiencies, were similar despite the varying amplitude of the modeled $[Ca^{2+}]_i$ spike under these conditions (*44*). A test of the sensitivity of the $Ca^{2+}$ sensor model (*22*) to the simulated $[Ca^{2+}]_i$ spikes revealed that simulated peak release rates were increased by 0.5 to 15% compared with the rates shown in Fig. 2C, which were calculated with rectangular $[Ca^{2+}]_i$ steps. The rate of release exhibited a similar $Ca^{2+}$ sensitivity when estimated with slower, flash lamp–evoked $Ca^{2+}$ uncaging (R. Schneggenburger and E. Neher, *Nature*, in press). In addition, uncaging $Ca^{2+}$ in a ramplike fashion with the monochromator produced release rates that were predicted by the model (J. H. Bollmann, unpublished observation).

16. To derive peak release rates from compound EPSCs, we simulated the time course of the release rate with a function of the form $f(t) = A\{1 + \mathrm{erf}[k_1 (t - t_0)]\} \exp[-k_2(t - t_0)]$, where erf is the error function. The convolution of this time course with the average quantal EPSC was fitted to the compound EPSCs in the interval from the onset to the peak of the EPSC by adjusting $A$, $t_0$, $k_1$, and $k_2$. This method takes the finite rise time (130 μs) of the average quantal EPSC into account.


17. H. Rosenboom and M. Lindau, *Proc. Natl. Acad. Sci. U.S.A.* **91**, 5267 (1994).
18. A. Tandon *et al.*, *Neuron* **21**, 147 (1998).
19. F. Helmchen, J. G. G. Borst, B. Sakmann, *Biophys. J.* **72**, 1458 (1997).


20. Because DM-nitrophen binds $Mg^{2+}$ well, $[Ca^{2+}]_i$ jumps to >15 μM were done in the absence of $Mg^{2+}$. In this case, ATP-dependent steps were not functional. However, in about half of the experiments with a $[Ca^{2+}]_i$ jump between 0.5 and 15 μM, the presynaptic solution contained $Na_2ATP$ (10 mM), GTP (0.3 mM), and $MgCl_2$ (3 mM), and therefore release in these experiments was not limited by the absence of MgATP (*45*). The $Ca^{2+}$ sensitivity was similar in these experiments, and they were included in Fig. 2, C and D. Despite the presence of MgATP, EPSCs in response to a second $[Ca^{2+}]_i$ jump were often reduced in size. Thus, most of the compound release data in Fig. 2, C and D are from the first laser pulse after terminal dialysis. In separate experiments ($n$ = 5), we verified that the releasable pool size did not change appreciably after terminal dialysis by comparing cumulative EPSC amplitudes in response to trains of afferent stimuli in the intact and dialyzed terminal.

21. The resting $[Ca^{2+}]_i$ before the flash affected the EPSC size and kinetics. In experiments in which the preflash Fura-2FF ratio exceeded $R_{min}$ by more than 1 SD (corresponding to a basal $[Ca^{2+}]_i \geq$ 300 nM), the normalized EPSC amplitude was reduced by ~50%, and the rise time was increased by ~20% compared with experiments in which the basal $[Ca^{2+}]_i$ was lower. These experiments were excluded from further analysis. Apart from partial pool depletion, possible mechanisms include adaptation of the $Ca^{2+}$ sensor (*31*) and an increase in the fraction of "reluctant" vesicles (*7*).

22. We used a sequential model to describe the binding of $Ca^{2+}$ to the $Ca^{2+}$ sensor ($X$):

$$X \underset{\beta}{\overset{5\alpha[Ca]}{\rightleftharpoons}} XCa_1 \underset{2\beta}{\overset{4\alpha[Ca]}{\rightleftharpoons}} XCa_2 \underset{3\beta}{\overset{3\alpha[Ca]}{\rightleftharpoons}} XCa_3 \underset{4\beta}{\overset{2\alpha[Ca]}{\rightleftharpoons}} XCa_4 \underset{5\beta}{\overset{\alpha[Ca]}{\rightleftharpoons}} XCa_5 \underset{\delta}{\overset{\gamma}{\rightleftharpoons}} XCa_5^*$$

The $Ca^{2+}$ binding (α) and dissociation (β) rate constants were 0.3 $\mu M^{-1}$ $ms^{-1}$ and 3 $ms^{-1}$, respectively ($K_d = \beta/\alpha$ = 10 μM). The $Ca^{2+}$ sensor was modeled to undergo a $Ca^{2+}$-independent isomerization step, similar to some existing $Ca^{2+}$-binding proteins [e.g., (*46*)]: A fully occupied sensor reversibly switches to a release-promoting state ($XCa_5^*$) with isomerization rate constants γ (30 $ms^{-1}$) and δ (8 $ms^{-1}$). Fusion of a vesicle was modeled in a second scheme in which the fusion rate constant is scaled by the fraction of $Ca^{2+}$ sensors that are in the release-promoting state:

$$V \xrightarrow{\rho XCa_5^*(t)} F.$$

ρ is the maximal fusion rate constant (40 $ms^{-1}$), $V$ the releasable vesicle, and $F$ the fused vesicle. The parameter $XCa_5^*(t)$ represents the fraction of $Ca^{2+}$ sensors promoting release at time $t$. As an important aspect of this model, the time course of the probability of release after an action potential depended little on the amount of $Ca^{2+}$ influx (*29*), because it was largely controlled by the $Ca^{2+}$-independent constants γ and δ. The differential equations derived from this reaction scheme were solved numerically (Mathematica 3.0). To obtain the time course of the EPSC, computed release rates were convolved with the time course of the measured quantal EPSC in the presence of CTZ ($n$ = 10 cells). The time course of the averaged quantal EPSC could be approximated with a rise time of 130 μs and a biexponential decay with time constants of 2.8 ms (54%) and 7.5 ms. $Ca^{2+}$ currents during an action potential were simulated with a Hodgkin-Huxley model (*47*). Resting $[Ca^{2+}]_i$ in intact terminals was assumed to be 50 nM (*19*). It was assumed that the $[Ca^{2+}]_i$ transients had the same time course as the $Ca^{2+}$ current and were identical at all release sites. The rationale behind these assumptions is our previous observation that many $Ca^{2+}$ channels contribute to the release of most vesicles during an action potential at the calyx of Held (*28*). This indicates that at most release sites, $[Ca^{2+}]_i$ cannot be expected to change faster than the presynaptic $Ca^{2+}$ currents.


23. P. Thomas, J. G. Wong, A. K. Lee, W. Almers, *Neuron* **11**, 93 (1993).
24. C. Heinemann, R. H. Chow, E. Neher, R. S. Zucker, *Biophys. J.* **67**, 2546 (1994).
25. P. Proks, L. Eliasson, C. Ämmälä, P. Rorsman, F. M. Ashcroft, *J. Physiol.* **496**, 255 (1996).
26. R. Heidelberger, C. Heinemann, E. Neher, G. Matthews, *Nature* **371**, 513 (1994).
27. R. H. Chow, J. Klingauf, E. Neher, *Proc. Natl. Acad. Sci. U.S.A.* **91**, 12765 (1994).
28. J. G. G. Borst and B. Sakmann, *Nature* **383**, 431 (1996).
29. W. M. Yamada and R. S. Zucker, *Biophys. J.* **61**, 671 (1992).
30. J. H. Bollmann, B. Sakmann, J. G. G. Borst, data not shown.
31. S.-F. Hsu, G. J. Augustine, M. B. Jackson, *Neuron* **17**, 501 (1996).
32. K. R. Delaney and R. S. Zucker, *J. Physiol.* **426**, 473 (1990).
33. R. Ravin, H. Parnas, M. E. Spira, N. Volfovsky, I. Parnas, *J. Neurophysiol.* **81**, 634 (1999).
34. C. Chen and W. G. Regehr, *J. Neurosci.* **19**, 6257 (1999).
35. D. D. Cummings, K. S. Wilcox, M. A. Dichter, *J. Neurosci.* **16**, 5312 (1996).
36. O. Ohana and B. Sakmann, *J. Physiol.* **513**, 135 (1998).
37. R. Robitaille, M. L. Garcia, G. J. Kaczorowski, M. P. Charlton, *Neuron* **11**, 645 (1993).
38. D. A. DiGregorio, A. Peskoff, J. L. Vergara, *J. Neurosci.* **19**, 7846 (1999).
39. H. Kasai, *Trends Neurosci.* **22**, 88 (1999).
40. J. G. G. Borst, F. Helmchen, B. Sakmann, *J. Physiol.* **489**, 825 (1995).
41. S. F. Traynelis, *J. Neurosci. Methods* **86**, 25 (1998).
42. E. Neher and R. S. Zucker, *Neuron* **10**, 21 (1993).

43. M. Naraghi, *Cell Calcium* **22**, 255 (1997).
44. Supplemental Web material is available at *Science* Online at www.sciencemag.org/feature/data/1052156.shl.
45. R. Heidelberger, *J. Gen. Physiol.* **111**, 225 (1998).
46. A. L. Hazard, S. C. Kohout, N. L. Stricker, J. A. Putkey, J. J. Falke, *Protein Sci.* **7**, 2451 (1998).
47. J. G. G. Borst and B. Sakmann, *J. Physiol.* **506**, 143 (1998).
48. Simulated delays were measured between the $[Ca^{2+}]_i$ jump and the time when the integral of the release rate equaled one vesicle. Delays predicted by the model were about 250 μs faster than the measured delays. $Ca^{2+}$ uncaging is too fast (10 to 20 μs) to contribute substantially to this additional delay (*11*, *12*). Therefore, it probably originates from processes downstream of $Ca^{2+}$ binding, including vesicle fusion, glutamate diffusion, and activation of AMPA receptors.

49. We thank C. J. Meinrenken, A. D. G. de Roos, and C. C. H. Petersen for comments on an earlier version of the manuscript; A. Roth for advice on simulations; and F. Helmchen for help with early flash photolysis experiments. J.G.G.B. was supported by a Pionier program of Netherlands Organization for Scientific Research (NWO).

12 May 2000; accepted 17 July 2000

# Uptake of Glutamate into Synaptic Vesicles by an Inorganic Phosphate Transporter

**Elizabeth E. Bellocchio,* Richard J. Reimer,* Robert T. Fremeau Jr., Robert H. Edwards†**

**Previous work has identified two families of proteins that transport classical neurotransmitters into synaptic vesicles, but the protein responsible for vesicular transport of the principal excitatory transmitter glutamate has remained unknown. We demonstrate that a protein that is unrelated to any known neurotransmitter transporters and that was previously suggested to mediate the $Na^+$-dependent uptake of inorganic phosphate across the plasma membrane transports glutamate into synaptic vesicles. In addition, we show that this vesicular glutamate transporter, VGLUT1, exhibits a conductance for chloride that is blocked by glutamate.**

Synaptic transmission involves the regulated exocytotic release of neurotransmitter. Because most classical transmitters are synthesized in the cytoplasm, they require transport into the secretory compartment for exocytotic release, and synaptic vesicles exhibit multiple distinct transport activities (*1*, *2*). All of these active transport processes depend on the proton electrochemical gradient ($\Delta\mu_{H+}$) across the vesicle membrane generated by the vacuolar $H^+$-dependent adenosine triphosphatase ($H^+$-ATPase) (*3*) and involve the exchange of lumenal protons for cytoplasmic transmitter. In particular, the transport of monoamines and acetylcholine (ACh) depends primarily on the chemical component ($\Delta$pH) of $\Delta\mu_{H+}$ (*4*, *5*), whereas the transport of glutamate depends predominantly on the electrical component ($\Delta\Psi$) (*6*, *7*). Accumulation of the inhibitory transmitters γ-aminobutyric acid (GABA) and glycine relies on both $\Delta$pH and $\Delta\Psi$ (*8*, *9*). Consistent with the observed differences in mechanism, the vesicular transporters for monoamines and ACh belong to a family of proteins distinct from the vesicular GABA transporter (VGAT) (*2*). VGAT shows greater dependence on $\Delta\Psi$ than do the vesicular monoamine and ACh transporters (*10*), suggesting that the vesicular glutamate transporter, which depends predominantly on $\Delta\Psi$, might belong to the same family of proteins defined by VGAT. Although several other proteins related to VGAT appear to have a role in the recycling of glutamate through glutamine at excitatory synapses (*11*–*14*), none have been implicated in vesicular glutamate transport.

The brain-specific $Na^+$-dependent inorganic phosphate transporter (BNPI) belongs to a family of proteins that use the inwardly directed $Na^+$ gradient across the plasma membrane to cotransport inorganic phosphate ($P_i$). Originally identified as a sequence upregulated by the exposure of cerebellar granule cells to subtoxic concentrations of *N*-methyl-D-aspartate, BNPI mediates the $Na^+$-dependent accumulation of $P_i$ in *Xenopus* oocytes (*15*). Additional work has implicated BNPI in adenosine 5′-triphosphate (ATP) production by neurons and protection against excitotoxic injury (*16*, *17*). However, BNPI is only expressed by glutamatergic neurons (*18*), militating against a general metabolic role in all neuronal populations. In *Caenorhabditis elegans*, genetic screens for multiple behavioral defects have identified mutants in the BNPI ortholog *eat-4* (*19*, *20*), and recent studies indicate a specific role for *eat-4* in glutamatergic neurotransmission (*21*). The glutamatergic defect in *eat-4* mutants appears to be presynaptic, consistent with the localization of BNPI to excitatory nerve terminals (*21*, *22*). The accumulation of cytoplasmic $P_i$ mediated by BNPI may activate the phosphate-activated glutaminase responsible for biosynthesis of the bulk of glutamate released as a neurotransmitter (*22*–*25*). However, the family of proteins including BNPI/EAT-4 may have functions in addition to $P_i$ transport.

BNPI shows sequence similarity to type I but not type II $Na^+/P_i$ cotransporters. In contrast to the type II transporters that exhibit robust $Na^+$-dependent $P_i$ uptake, the accumulation of $P_i$ by type I transporters is less striking (*26*-*28*). Rather, the type I transporter NaPi-1 transports organic anions, including phenol red and penicillin G, with substantially higher apparent affinity than $P_i$ (*28*). Human genetic studies have shown that mutations in another protein closely related to BNPI and NaPi-1 account for disorders of sialic acid storage (*29*). In these conditions, sialic acid accumulates in lysosomes because of a defect in proton-driven export (*30*–*33*). Although the sialin protein (*29*) has not been demonstrated to mediate sialic acid transport, these observations together with the report that NaPi-1 accumulates organic anions with high apparent affinity suggest that BNPI might also transport organic anions. Localization to glutamatergic nerve terminals raises the possibility that it transports glutamate. In addition, BNPI is localized to synaptic vesicles in the brain (*22*) and to intracellular membranes in transfected cells (*34*), suggesting a role for BNPI in the transport of glutamate into synaptic vesicles for regulated exocytotic release. To determine whether BNPI mediates the transport of glutamate into synaptic vesicles, we transfected the rat BNPI cDNA into rat pheochromocytoma PC12 cells (*35*), which lack detectable endogenous BNPI protein (*34*). We then prepared a population of light membranes, including synaptic-like microvesicles, from the transfected and untransfected cells (*10*) and tested their ability to accumulate $^3$H-glutamate in the presence of 4 mM chloride and ATP (*36*), conditions that optimize glutamate accumulation by native synaptic vesicles (*6*, *7*). Membranes from the transfected cells exhibited an uptake of glutamate that was two to four times the uptake by membranes from

Departments of Neurology and Physiology, Graduate Programs in Neuroscience, Cell Biology, and Biomedical Sciences, University of California at San Francisco School of Medicine, 513 Parnassus Avenue, San Francisco, CA 94143–0435, USA.

*These authors contributed equally to the work.
†To whom correspondence should be addressed. E-mail: edwards@itsa.ucsf.edu